Hindawi Publishing Corporation
Journal of Nanomaterials
Volume 2011, Article ID 317673, 17 pages
doi:10.1155/2011/317673

Review Article

Design Modifications in Electrospinning Setup for Advanced Applications

Rahul Sahay,[1,2] Velmurugan Thavasi,[1] and Seeram Ramakrishna[1]

[1] *NUS Nanoscience and Nanotechnology Initiative, National University of Singapore, Singapore 117576*
[2] *School of Materials Science and Engineering, Nanyang Technological University, 50 Nanyang Avenue, Singapore 639798*

Correspondence should be addressed to Velmurugan Thavasi, velnanotech@gmail.com

Received 12 July 2011; Accepted 28 August 2011

Academic Editor: Yanqiu Zhu

The paper deals with the modification made to the general electrospinning setup. The emphasis is given to characterize the designs based on their applicability. Four basic categories are identified, namely, patterned fibers, fiber yarns, multicomponent, and deposition area of the fiber mat obtained. The mathematical modeling to better understand the physics behind the modification made to the general electrospinning setup is presented. Emphasis is given to critically analyse these categories on the basis of the applications served by them. Each of these categories is found to serve a specific poll of advanced application enabling the researchers to make a calculated choice for the design of the electrospinning setup for particular application.

1. Introduction

Electrospinning is one of the most widely used processes for the production of nanofibers. This technique of producing nanofibers employs electrostatic forces for stretching the viscoelastic fluid. The fiber diameters obtained are found to be one or two orders of magnitude smaller than the conventional spinning techniques. As the process is capable of achieving large surface to volume ratios with desirable physical and chemical properties, it has been considered for a wide variety of applications, ranging from sensors [1], antibacterial surfaces [2], scaffolds [3], photocatalyst [4], nanofilters [5], anti-counterfeiting application [6], water-proof fabric [7], and solar energy applications [8].

Electrospinning is a simple process employing a syringe pump, high voltage direct current (HVDC) supply, and a grounded collector. The syringe pump connected to the syringe is employed to control the flow rate of the polymer solution as depicted in Figure 1. HVDC power supply is connected to the metallic needle. This metallic needle, on the other hand, is connected to the syringe. When the high voltage is applied to a polymer drop emanating from the metallic needle, the charged particles start to concentrate on the surface of the polymer drop, thus resulting in the excess buildup of charged particles at the tip of the drop. At some critical value of the applied electric field proposed by Taylor [9], applied electric field surpasses the surface tension and results in jetting from the polymer drop. The trajectory of polymer jet is a straight line before it starts to curl and spiral in space. This curling and spiraling of polymer jet are responsible for the reduction of its diameter to the order of nanometers resulting in nanofibers as depicted in Figure 2. These fibers later get deposited on the grounded surface. It is advisable to make a brief note of the mathematical modeling pertaining electrospinning as it will help to better understand the physics behind the modification made to the general electrospinning setup.

2. Mathematical Modeling of the Electrospinning Process

Although vast majorities of work related to electrospinning were of an experimental nature, nevertheless, some theoretical studies had been proposed. The theoretical studies could be divided into two broad categories. The first category dealt with the mathematical analysis related to straight section of electrospun jet. On the other hand, the second category was related to the bending instabilities suffered by the electrospun jet. Spivak et al. [10, 11] proposed a one-dimensional (1D)

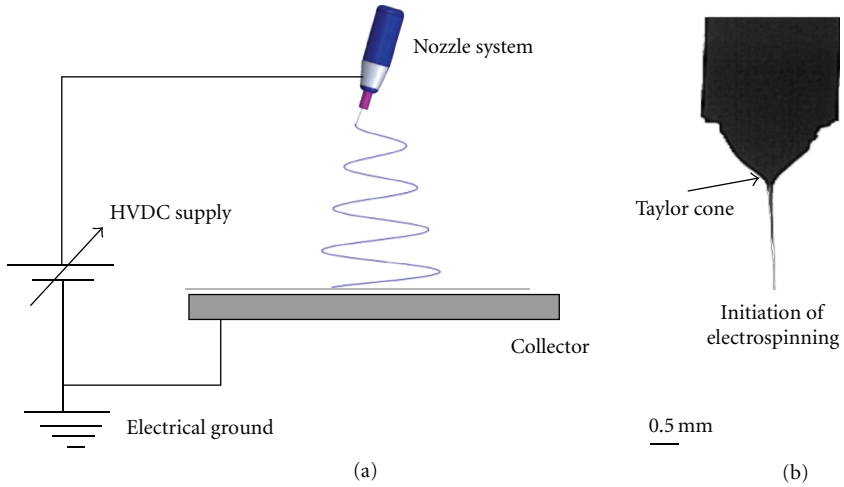

Figure 1: (a) The schematic of basic electrospinning. The nozzle system usually consists of a needle and a syringe pump. Where HVDC stands for high voltage direct current. (b) The figure depicts the formation of Taylor cone required for the initiation of electrospinning. The images were obtained with the help of high speed camera at 2000 f/s.

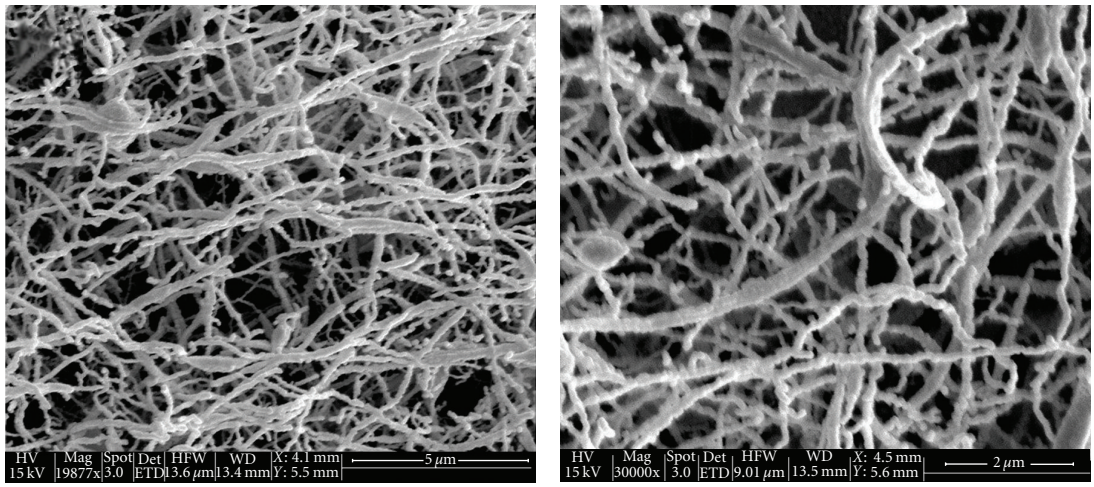

Figure 2: CuO fibers fabricated through electrospinning. (a) Composite fibers: the chemical reagents (copper acetate and water) were dissolved in 10 wt% aqueous poly(vinyl) alcohol solution. The polymer solution was employed to achieve appreciable viscosity required for the initiation of electrospinning. The electrospinning was performed at flow rate of 0.25 mL/h with the applied electric field strength of 1.33 kV/cm. (b) Annealed fibers: the composite fibers obtained were annealed at 500°C to remove polymer as water vapor and CO_2 resulting in pure CuO fibers.

model for the electrospun jet, with fluid behavior represented by a nonlinear power law rheological constitutive equation. Yarin et al. [12, 13] modeled the jet as a series of charged beads connected by viscoelastic dumbbell elements. Hohman et al. [14, 15] proposed a model, which accounted for the influence of the charge density of the jet on the surrounding electric field. The fluid employed, was considered as Newtonian in nature. Feng [16, 17] reformulated the Hohman et al. treatment, accounting for viscoelastic polymeric rheological behavior. The viscoelastic behavior was employed by incorporating the Giesekus constitutive equation into the jet-governing equations. Carroll and Joo [18] modeling of the electrospinning process closely followed the work of Feng, with the introduction of Oldroyd-B and FENE-P constitutive equations for modeling the rheological behavior of Boger fluids.

The second phase of electrospinning had been studied by Reneker et al. [19]. They proposed that the electrically driven bending instabilities of an electrospun jet as the particular case of the general Earnshaw theorem in electrostatics. On the other hand, Hohman et al. [14] proposed instability models to describe the phenomena observed during electrospinning. Models related to higher order instabilities such as "branches on electrospun jet" was also proposed by Yarin et al. [20].

2.1. Straight Section of Electrospun Jet. Spivak et al. [10, 11] modeled the motion of a weakly conductive infinite viscous

jet accelerated by an external electric field taking into account the inertial, hydrostatic, viscous, electrical, and surface tension forces. The polymer fluid was described by a nonlinear power law rheological constitutive equation. The linear momentum, mass, and electric charge conservation equations were obtained by averaging over the jet cross-section to give the resultant equation along the jet flow direction. The asymptotic momentum equation in its dimensionless form was given by the expression

$$\left\{\widetilde{R}^{-4} + We\widetilde{R}^{-1} - Y\widetilde{R}^{2} - \frac{1}{\mathrm{Re}}\left(\frac{1}{2}\frac{d}{d\widetilde{z}}\left(\widetilde{R}^{-2}\right)\right)^{m}\right\} = \widetilde{Z} + \mathrm{C}, \tag{1}$$

where dimensionless jet radius $\widetilde{R} = R/R_0$, where R_0 was the characteristic jet radius. Dimensionless axial coordinate $\widetilde{Z} = Z/Z_0$, where $Z_0 = \rho Q^3/2\pi^2 R_0^4 E_0 I$. The nondimensional parameters were Weber number $We = (2\pi^2 R_0^3 \sigma_s)/(\rho Q^2)$ represented the ratio of the surface tension forces to the inertial forces. $Y = \pi^2 I^2 R_0^6/(4\varepsilon_0 \rho Q^4)$ represented the ratio of the electrical to inertial forces. The effective Reynolds number for the fluid is given by $\mathrm{Re} = (Q^2\rho)/(2\pi^2 R_0^2 \mu)\,[4\pi E_0 I R_0^2/(Q^2\rho)]^{-m}$. All the symbols have their usual meaning, and m is the flow index in the rheological constitutive equation. The constant C was evaluated with the help of the imposed boundary conditions. Substituting power law asymptotic approximation of the jet radius ($\widetilde{R} \sim \widetilde{z}^{-\alpha}$) in the integrated form of the asymptotic momentum equation (1) results

$$\widetilde{z}^{-4\alpha} + We\widetilde{z}^{-1\alpha} - Y\widetilde{z}^{-2\alpha} - \frac{\alpha^m}{\mathrm{Re}}\widetilde{z}^{(2\alpha-1)m} - \widetilde{Z} = O(1). \tag{2}$$

Spivak et al. [10, 11] numerically integrated asymptotic momentum (2) and compared it with the experimental measurements obtained for a 4 wt% aqueous solution of poly(ethylene) oxide ($M_w = 1,450,000$) electrospun at an electric field strength of 0.4 kV/cm. Spivak et al. [10, 11] observed good agreement between numerical and experimental values over a distance of 15 mm from the initiation of the spinning process.

Yarin et al. [12, 13] derived quasi-one-dimensional equations for the conservation of mass, momentum, and electrical charge describing the dynamics of the electrospun jet

$$\lambda f = \lambda_0 f_0, \tag{3}$$

$$\begin{aligned}\rho\lambda_0 f_0 \frac{\partial V}{\partial \tau} &= \tau\frac{\partial p}{\partial s} + \lambda|\kappa| pn - \rho_g \lambda_0 f_0 k \\ &\quad + \lambda|\kappa| \times \left(\pi a\sigma - e^2 \ln\frac{l}{a}\right)n - \lambda_\varepsilon \frac{U_0}{h}k,\end{aligned} \tag{4}$$

$$e\lambda = e_0\lambda_0, \tag{5}$$

where "s" was a Lagrangian parameter "frozen" into the jet elements. Equation (3) represents conservation of mass, where λ was the geometrical stretching ratio such that $\lambda ds = d\zeta$, and the $f = \pi a^2$ being the cross-sectional area. Subscript zero denotes the parameter values at the time $t = 0$. Equation (4) was momentum balance equation with ρ being the liquid density, V its velocity, p the longitudinal force in the jet cross section, and g is acceleration due to gravity. U_o being the value of electrical potential at the jet origin and "h" the distance between the origin and the collecting plate. Equation (5) represents the conservation of charges. In Cartesian coordinates, the kinematics relations were given as $\partial R/\partial\tau = V$, where R was the radius vector of a point on the axis of the jet. Substituting the kinematics relations in (4), a system of scalar equations was obtained. The simplest version of the upper-convected Maxwell model of viscoelasticity was assumed to describe the behavior of electrospun jet. This system of the equations allowed Yarin et al. to obtain the jet configuration in space at any particular instance of time. Comparisons were made between experimental and theoretical results for a 6 wt% poly(ethylene) oxide solution dissolvent in 60/40 v/v water/ethanol mixture. The applied electric field strength was 1 kV/cm. The predicted motion of the jet was found to be in good agreement with the experimental data until about 3 ms after jet initiation.

Hohman et al. [14, 15] modeled the electrospinning process based on the approach that the instabilities occurred on a length scale much longer than the jet radius. As a result, the jet was represented as a long, slender object. The polymer fluid was considered Newtonian and incompressible. The three-dimensional variables considered were radial velocity (V_r), axial velocity (V_z), radial electric field (E_r), and axial electric field (E_z). Taylor series expansions in r (instantaneous radius of the jet) of these four variables were substituted into three-dimensional equations for conservation of mass, conservation of charge, and momentum balance. Only the leading terms of the expansions were retained. The resulting hydrodynamic equations were made nondimensional by employing length scale r_0, where r_0 was the diameter of the capillary; time scale $t_0 = \sqrt{\rho r_0^3/\gamma}$, where γ was the surface tension and ρ was the density of the fluid; an electric field strength $E_0 = \sqrt{\gamma/(\varepsilon - \bar{\varepsilon})}r_0$, where ε and $\bar{\varepsilon}$ were the permittivity of the fluid and air, respectively, and surface charge density was given by $\sqrt{\gamma/(\bar{e})}/r_0$. The material properties of the fluid were characterized by dimensionless parameters $\beta = \varepsilon/\bar{\varepsilon} - 1$, the dimensionless viscosity $\nu^* = \sqrt{\nu^2/(\rho\gamma r_0)}$, the viscous scale $l_\nu = \rho\nu^2/\gamma$. The other nondimensional parameters are dimensionless gravity $g^* = g\rho r_0^2/\gamma$ and the dimensionless conductivity $K^* = K\sqrt{\rho r_0^3/(\beta\gamma)}$. The nondimensionalized equations for conservation of mass and charge and the Navier-Stokes equation for the conservation of momentum were given as follows:

$$\begin{aligned}\partial_t(h^2) + (h^2 v)' &= 0, \\ \partial_t(\sigma h) + \left(\sigma h v + \frac{K^*}{2}h^2 E\right) &= 0, \\ \partial_t v + v v' &= -\left(\frac{1}{h} - h'' - \frac{E^2}{8\pi} - 2\pi\sigma^2\right) \\ &\quad + \frac{2\sigma E}{h\sqrt{\beta}} + g^* + \frac{3\nu^{*2}}{h^2}(h^2 v')',\end{aligned} \tag{6}$$

where $h(z)$ was the radius of the jet at axial coordinate z; $V(z)$ was the axial velocity of the jet and was assumed to be constant across the jet cross-section; $\sigma(z)$ was the surface charge density; $E(z)$ was the electric field in the axial direction. The prime on the variables denotes differentiation with respect to z. The nondimensionalized tangential field inside the jet, was expressed as

$$E = E_\infty + \int ds \frac{\lambda(s)}{|x - r(s)|} \approx E_\infty + \ln \frac{r}{L}\left(\frac{\beta}{2}(h^2E)' - \frac{4\pi}{\bar{\varepsilon}}h\sigma\right), \tag{7}$$

where $\lambda(s)$ was the linear charge density along the jet, parameterized by the arc length "s," which varied over the length scale "L" much larger than the jet radius.

Feng [16, 17] simplified the Hohman et al. [14, 15] formulation by making it insensitive to the initial charge density, except inside a tiny "boundary layer" at the capillary end. They integrated viscoelastic polymeric rheological behavior by incorporating the Giesekus constitutive equation into the governing equations given as

$$\frac{\overline{\eta}^+}{3\eta_s} = \left\{\frac{\exp\{p[1 - \cos(\gamma^2/\gamma_s^2)]\} \text{ if } \gamma \le \gamma_s}{\exp(2p) \text{ if } \gamma \le \gamma_s}\right\}. \tag{8}$$

The governing equation for the unknown parameters R, v, E, and σ were given by the (9)–(12). The characteristic qualities length R_0, velocity $v_0 = Q/(\pi R_0^2)$, electric field $E_0 = I/(\pi R_0^2 k)$, and surface charge density $\sigma_0 = \bar{\varepsilon}E_0$ were used for scaling the governing equations. The resultant governing equations were

$$vR^2v = 1, \tag{9}$$

$$R^2E + PeRv\sigma = 1, \tag{10}$$

$$vv' = \frac{1}{Fr} + \frac{3}{\mathrm{Re}\,R^2}\frac{d}{dz}(\eta R^2 v') + \frac{1}{We}\frac{R'}{R^2} + \Xi\left(\sigma\sigma' + \beta EE' + \frac{2\sigma E}{R}\right), \tag{11}$$

$$E = E_\infty - \ln\chi\left(\frac{d(\sigma R)}{dz} - \frac{\beta}{2}\frac{d^2(ER^2)}{dz^2}\right), \tag{12}$$

where the nondimensional groups are given as $Fr = v_0^2/gR_0$, $Pe = 2\bar{\varepsilon}v_0/KR_0$, $\mathrm{Re} = \rho v_0 R_0/\eta_0$, $We = \rho v_0^2 R_0/\gamma$, $E = \bar{\varepsilon}E_0^2/\rho v_0^2$, $De = \lambda v_0/R_0$, $r_\eta = \eta_p/\eta_0$, and $\beta = \varepsilon/\bar{\varepsilon} - 1$, $\chi = L/R_0$. The other symbols have their usual meaning. Feng [16, 17] documented that strain hardening promoted jet thinning at the beginning but suppressed it further downstream to produce thicker fibers. In addition, the Giesekus model also predicted earlier onset of strain hardening at higher strain rate. Though definitive comparisons with experiments were not performed, the theory appeared to predict jet thinning on the right order of magnitude.

Carroll and Joo [18] modeled the electrospinning process that closely followed the work of Feng [16, 17]. The model consisted of steady state equations for mass, charge, momentum conservation, as well as an electric field equation with the introduction of Oldroyd-B and FENE-P constitutive equations for modeling the rheological behavior of Boger fluids. The nondimensional governing equations were

$$vR^2v = 1, \tag{13}$$

$$R^2E + PeRv\sigma = 1, \tag{14}$$

$$vv' = \frac{1}{Fr} + \frac{3}{\mathrm{Re}\,R^2}\frac{d}{dz}(\eta R^2 v') + \frac{1}{We}\frac{R'}{R^2} + \Xi\left(\sigma\sigma' + \beta EE' + \frac{2\sigma E}{R}\right), \tag{15}$$

$$E = E_\infty - \ln\chi\left(\frac{d(\sigma R)}{dz} - \frac{\beta}{2}\frac{d^2(ER^2)}{dz^2}\right). \tag{16}$$

For the special case of the infinitely extensible polymer chain, the polymeric stress components reduce to the Oldroyd-B model were

$$\tau_{pzz} + De\left(v\tau'_{pzz} - 2v'\tau_{pzz}\right) = 2(1 - B)v', \tag{17}$$

$$\tau_{prr} + De\left(v\tau'_{prr\,pzz} + v'\tau_{prr}\right) = -(1 - B)v'. \tag{18}$$

The momentum and electric field equations, (15) and (16), were both second order ordinary differential equations, which were rewritten as a set of four first order ODEs. The polymeric stress (17) and (18) add two first order ODE. To solve this system of equations, six boundary conditions were formulated as also performed by Feng [16, 17]. Carroll and Joo [18] demonstrated that the one-dimensional model for electrically driven jet had correctly captured the initial straight-line motion of jet. The resultant simulation had given good quantitative jet radius profiles plotted against parameters such as the electrical conductivity, fluid viscoelasticity, and volumetric flow rate, which were in good agreement with experimental results.

2.2. Bending Instabilities of Electrospun Jet. Reneker et al. [19] considered the electrically driven bending instabilities of an electrospun jet as the particular case of the general Earnshaw theorem in electrostatics. The theorem states that it is impossible to create a stable structure in which the elements interact only by Coulomb's law. The result of the phenomenon will be a lateral force component that will cause the jet to deviate from its original initiated path into a looping spiraling trajectory.

Hohman et al. [14, 15] performed linear instability analysis to better understand the phenomenon of bending instabilities of the electrospun jet. Three different types of instabilities were predicted, two of which were axisymmetric whereas, third was non-axisymmetric in nature. The first axisymmetric mode was stated to be associated with the Raleigh instability, which was dominated by surface tension. The Raleigh instability was suppressed at high electric fields and was considered irrelevant for electrospinning. The other two modes were electrically driven and referred to as "conducting" modes. These conductive modes were primarily sensitive to fluid conductivity and insensitive to surface tension at high electric fields. The one of these conductive modes was

axisymmetric, while the second was non-axisymmetric in nature. The competition between the two conducting modes was of importance at high electric fields of the electrospinning process. The mode that will dominate depends on both the surface charge density and the radius of the jet as it thins away from the tip of the needle.

3. Effect of Applied Forces on the Trajectory of Electrospun Jet

Although the electrostatic force is the dominant force experienced by the electrospun jet, it is beneficial to compare qualitatively the forces acting on the electrospun jet. As can be seen from (12) and (16), the electric field acting on the jet in the axial direction is the sum of external applied electric field and the electric field induced by the total free charge on the jet surface. The total free charge on the jet is given by the (10) and (14). This total charge is the sum of conductive and convective charges. It is observed that conductive charge transfer dominates the charge transfer mode inside the Taylor cone [12]. This conductive charge gives way to convective charge as the jet thins away from the Taylor cone to the collector surface. This implies that contribution to the total electric field from the free charge reduces as the jet moves away from the needle exit. This implies that the total electric field near the collector surface is approximately same to the external applied electric field. This is theoretically an order of magnitude reduction in the total electric as the jet moves from the needle tip to the collector surface.

The total electric field can be increased either by increasing the external applied electric field or by increasing the total charge density. Salt (NaCl) is considered as one of the widely used additive to increase the charge density of the polymer solution [21]. The other additives used for increasing the charge density are ionic surfactant [22], which has the dual purpose of increasing the conductivity while reducing the surface tension of the polymer solution. This increase in the charge density, as predicted by Hohman et al. [14, 15], will aggravate non-axisymmetric instabilities colloquially known as the bending instabilities making it difficult to control the trajectory of the jet.

For the initiation of electrospun jet the electrostatic force has to overtake surface tension. This happens at the tip of the Taylor cone, where charge density is the maximum. Ironically, the surface tension is maximum at the tip of the Taylor cone due to the infinitesimally small radius at the tip. This large charge density at the tip of Taylor cone increases the total electric field by an order of magnitude greater than the applied electric field, thus enabling the initiation of the jet from the tip of Taylor cone. After the initiation of electrospun jet, high viscoelastic force of polymer jet suppresses the surface tension, resulting in uniform diameter electrospun jet. Surface tension becomes relevant again with the decrease in the jet radius as the jet thins away from the metallic needle to the collector surface. In cases where the surface tension surpasses viscoelastic forces, it results in the formation of beads [23]. The beads are the local increase in the jet diameter, which results from axisymmetric nonconducting instability better known as Rayleigh Plateau instability [24]. Beads are considered as defects as it reduces the large surface area of the electrospun fibers as shown in Figure 3. Increase in the free charge density results in an increase in the stretching of jet and thus reduces the bead formation [25]. Increase in the viscoelastic forces by increasing the viscosity [26] of the polymer solution is the other way of surpassing bead formation. The viscosity of the polymer solution can be increased by either increasing the molecular weight or concentration of the polymer solution. Nevertheless, beaded fibers were obtained with an increase in the polymer concentration in case of polymer blend as shown in Figure 4. This may be due to the nonlinear interaction of polymer component in the polymer blend resulting in variable viscosity profile.

Inertia and aerodynamic drag force were considered negligible in comparison to electrostatic force during the initiation of electrospun jet from a polymer drop. Upward needleless electrospinning [27] is one of the examples which confirms the given argument. Nevertheless, these forces (aerodynamic drag and inertia) start to become significant as the jet gets close to the collector surface due to the reduction of total electric force near the collector surface as discussed earlier. For instance, the fiber mat collected by the upward electrospinning setup will be more porous and loosely bound together as compared to the normal electrospinning setup due to the inertial effect of nanofibers. These forces (aerodynamic drag and inertia) also tend to play an important role during the patterning of electrospun jet. For instance, the most common collector device used for the collection of aligned fibers is the rotating mandrel. As the electrospun jet comes near to the fast rotating mandrel, it experiences a drag force due to the rapid displacement of air near the mandrel surface, which affects its alignment. The analysis pertaining to the drag force experienced by the electrospun jet due to the rotating mandrel will appear elsewhere.

4. Need for Modifications in the Electrospinning Setup

It has been observed that the electrostatic force is the driving force behind the bending instability of electrospun jet. This bending instability is responsible for the reduction of jet diameter to the order of nanometer. This particular instability is also responsible for the randomness of the resultant product obtained. This makes it obvious that manipulating electric field lines will help to control the trajectory of the electrospun jet and so does the architecture of the final product.

Possible configurations of electric field lines between the needle system and the collector are shown in Figure 5. From herein and hereafter the term "needle system" will comprise of the syringe pump, HVDC supply, and metallic needle connected to the syringe. Figure 5(a) shows the electric field lines for point-plate system. Here, "point" is represented by the needle system, whereas "plate" is the infinitely long collector surface with respect to the needle system. These electric field lines depict the configuration for general electrospinning setup. In practice, the "plate" collector configuration can be

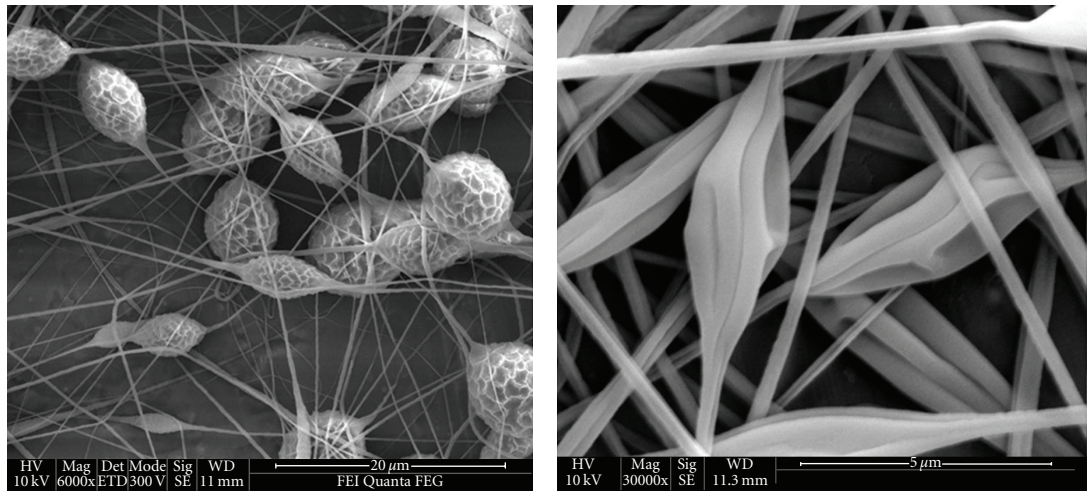

(a) (b)

Figure 3: Formation of beads on electrospun fibers prepared using 10% polyvinyl pyrrolidone (PVP) dissolved in dimethylformamide (DMF) with the applied electric field strength of 2.0 kV/cm.

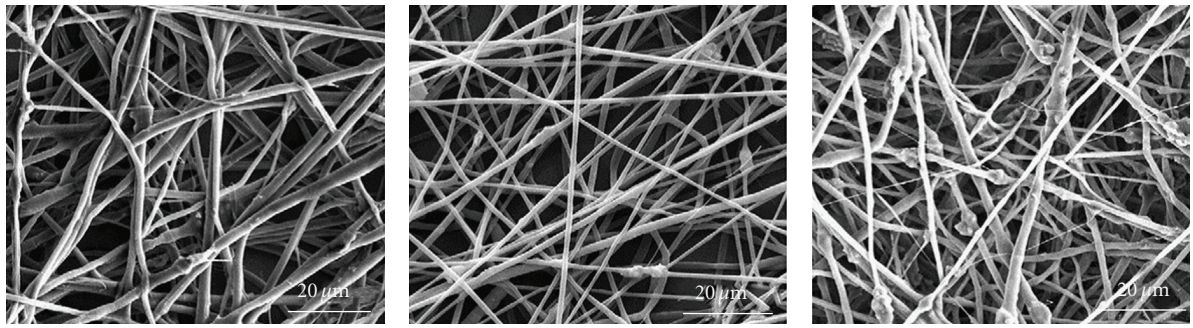

(a) (b) (c)

Figure 4: The figure depicts the effect of the concentration of the polymer solution on fiber morphology. The fibers were fabricated from poly(ethylene) oxide (PEO) blended with (a) 6%, (b) 12%, and (c) 19% PANi. The blended polymer was dissolved in chloroform. The electrospinning was performed at flow rate of 0.3 mL/h with the applied electric field strength of 1.25 kV/cm.

represented by a conducting plate, rotating mandrel, and so forth. Figure 5(b) shows electric field lines for point-point system. Here, the "point" collector represented by sharp-pointed surfaces. These surfaces may include a tip of a sharp pointed knife, sharp edges of plate, thin metallic wires, and so forth. As it seems from the Figure 5(b), the purpose of point collector is to concentrate the electric field lines and thus the trajectory of the jet at an infinitesimally small point. Figure 5(c) depicts the highly uniform electric field lines for plate-plate system. This setup though will produce a uniform jet profile is seldom employed as it requires higher externally applied electric field strength as compared to the point-plate system for the initiation of electrospinning.

As will be seen later, the large number of electrospinning setups employ components to concentrate electric field lines at a certain given point or a given area. This confinement, though helps in achieving controlled deposition of nanofibers, hinders the possible trajectory of electrospun jet. This hindered trajectory of electrospun jet will subsequently hinder the reduction of jet diameter as it moves from the needle tip to the collector surface. It is noted later during the discussion of electrospinning setups that this phenomenon resulted in micron or submicron diameter fibers. Nevertheless, these possible configurations of electric field lines will help us in understanding the mechanism behind the fiber alignment.

In this paper, the emphasis has been given to characterize the configurations of electrospinning setups on their usage. This is done to help the reader make a calculated choice regarding design of their electrospinning setup. Four basic categories were identified, namely, patterned fibers, fiber yarns, and multicomponent and rate and area of deposition of electrospun mat.

4.1. Patterned Fibers. The patterning of nanofibers was found important as ordered architecture finds applications in fields such as electronics [28], skeletal muscle regeneration [29], and polarized luminescence [30]. These configurations

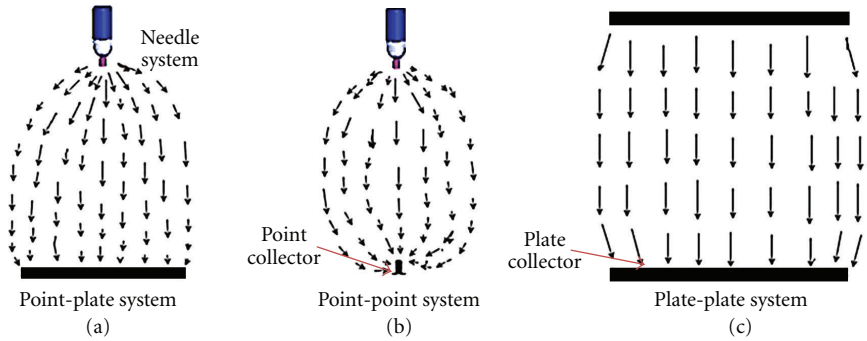

Figure 5: Possible configurations of electric field lines between the needle system and the collector.

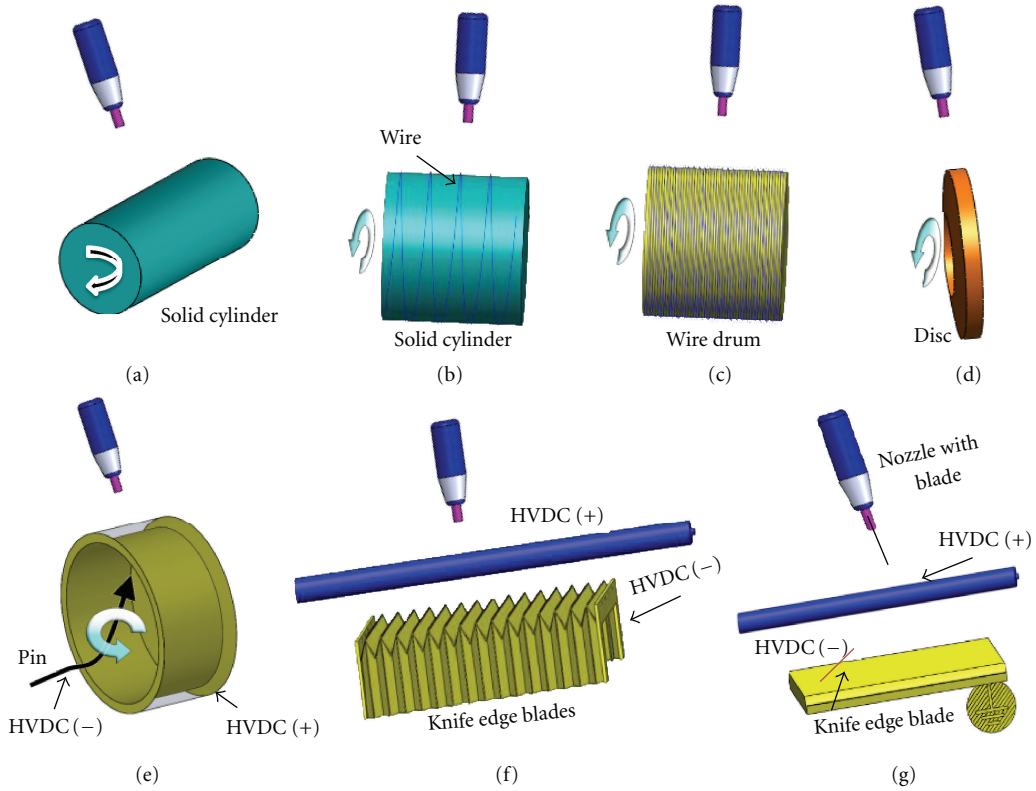

Figure 6: Category of electrospinning setups based on rotating device. These configurations include (a) solid cylindrical, (b) wire winded on an insulated cylinder, (c) wired drum, (d) disc collector, (e) sharp pin inside the rotating collector, (f) knife-edged electrodes, and (g) knife-edged electrode and needle system.

include 1D- as well as 3D-aligned structures. Other specific-patterned structures have been configured so as to fulfill the desired requirements. The configurations can be broadly divided based on the manipulations in the subsystems. These subsystems include the needle system and the collector. The collector can be further divided into the rotating device or a configuration of electrodes.

The major category of electrospinning setups configuring aligned nanofibers employs a rotating device as the collector. The purpose of the rotating device is to mechanically stretch the fibers, thus helping it to align along the periphery of the mandrel. The mandrel can transverse along its axis in order to obtain aligned fiber mat. These configurations include a solid cylindrical collector [31], which can rotate about its axis, shown in Figure 6(a). The aligned fibers obtained with the help of solid rotating drum are shown in Figure 7. The other variations include a conducting wire wound on an insulated cylinder by Bhattarai et al. [32] as shown in Figure 6(b). These conducting wires act as the electric field concentrator as shown in Figure 5(b). As expected, a highly aligned fiber bundle was obtained on and in near vicinity of wires. It was also noted that the size of the fiber bundle directly correlates with the thickness of the wire. Similarly, in case of wired drum [33] in Figure 6(c), each wire acts as the electric field concentrator, resulting in aligned fiber at the low speed of the drum. On the similar lines, Sundaray et al. [34]

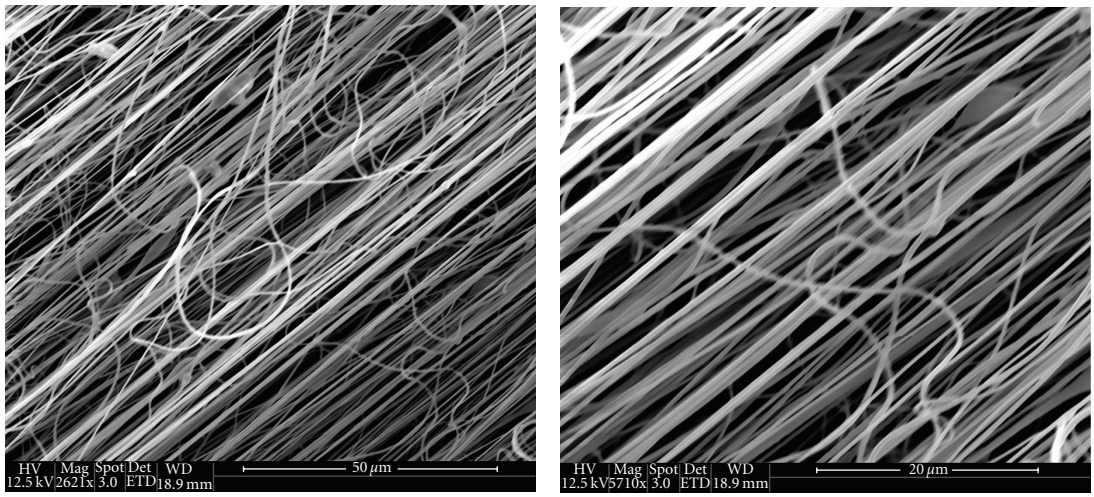

(a) (b)

Figure 7: Aligned nanofibers of 10 wt% polyacrylonitrile (PAN) dissolved in dimethylformamide (DMF) collected on a rotating drum. The rotation speed of the drum was kept at 2000 rpm. The electrospinning was performed at the flow rate of 1.2 mL/h with the applied electric field strength of 1.5 kV/cm.

placed a sharp pin inside the rotating collector as an electric field concentrator shown in Figure 6(e). As the drum was given translational motion, it resulted in large deposition area of the aligned nanofibers. Nevertheless, cross-bar pattern (instead of uniaxially aligned fibers) is resulted due to the translation motion of the drum. Other configurations employing electric field concentrator include knife-edged electrodes (Figures 6(f) and 6(g)) employed by Teo et al. [35, 36]. Appreciable degree of alignment was obtained with the provisions to control the direction of aligned fibers. One of the of the notable collector configurations based on disc collector [37] depicted in Figure 6(d), is Zussman et al.'s [38] collector system. The collector system consists of rotating disc and a small aluminum table attached to the disk edge. Double- and triple-layer highly aligned crossbar structures were obtained. The only drawback of the setup was the manual rotation of aluminum table for the deposition of the subsequent nanofibrous array. Similar setup was designed in the laboratory to fabricate aligned fibers as shown in Figure 8(a). It was noted that alignment of the fibers improved with an increase in the rotation speed of the disc from 800 rpm (Figure 8(b)) to 2000 rpm (Figure 8(d)).

The collector configurations shown in Figure 9 are based upon a group of counter electrodes placed in certain configuration. Appreciable degree of alignment was obtained from these proposed setups. Figures 9(a) and 9(b) show a setup consisting of parallel electrodes and an array of counter electrodes designed by Li et al. [39, 40], as expected edges of electrodes act as the electric field concentrator. These electric field concentrators thereby exert tensional electrostatic force on electrospun jet resulting in the stretching of the jet to the linear array between two given edges. On the similar lines, Teo and Ramakrishna [35] configured the collector system from two steel blades placed with a gap between them, shown in Figure 9(c). This system enabled to align fibers between the tip of steel blades. It was also observed that the postprocessing resulted in the improvement of the alignment of the electrospun fibers. Similarly, Lee et al. [41] designed a collector system composed of two pieces of conductive substrates separated by a gap. This particular setup helped to obtain uniaxial aligned fibers between the gap. On the similar lines, Kakade et al. [42] employed a set of electrically charged aluminum plates with a variable gap as a collector. The electrical polarity of the aluminum plates was kept negative with respect to the one applied to the syringe system. Kakade et al. [42] successfully aligned nanofibers between two electrically charged aluminum plates. Similarly, Shin et al. [43] designed a parallel electrode system consisting of aluminum and gold electrodes as shown in Figure 9(d) to obtain aligned fiber mat. The gold electrodes were patterned to have a single trench placed between a pair of subelectrodes. The subelectrodes made of a rectangular aluminum foil and insulating plates were placed parallel to each other. Both the main collectors and the subelectrodes were grounded.

Although these configurations can achieve a high degree of orientation in nanofibers, they suffer from the low throughput as compared to rotating drum. Kakade et al. [42] compared the aligned fibers obtained from a rotating mandrel with the fibers collected between the electrically charged plates. It was noted that polymer chains within the nanofibers were oriented only in case of electrically charged plates. The electric charge on the aluminum plates was found to be responsible for the phenomenon as compared to the grounded mandrel.

The particular setup shown in Figure 9(e) consists of the usual needle system consisting of a syringe pump and HVDC supply connected to a metallic needle. The collector for this particular setup consists of two pieces of stainless steel collectors (collector 1 and collector 2). The provision was made in the setup to selectively connect the collectors to HVDC power supply. This particular provision helped Ishii et al. [44] obtain straight fiber forms between the collectors.

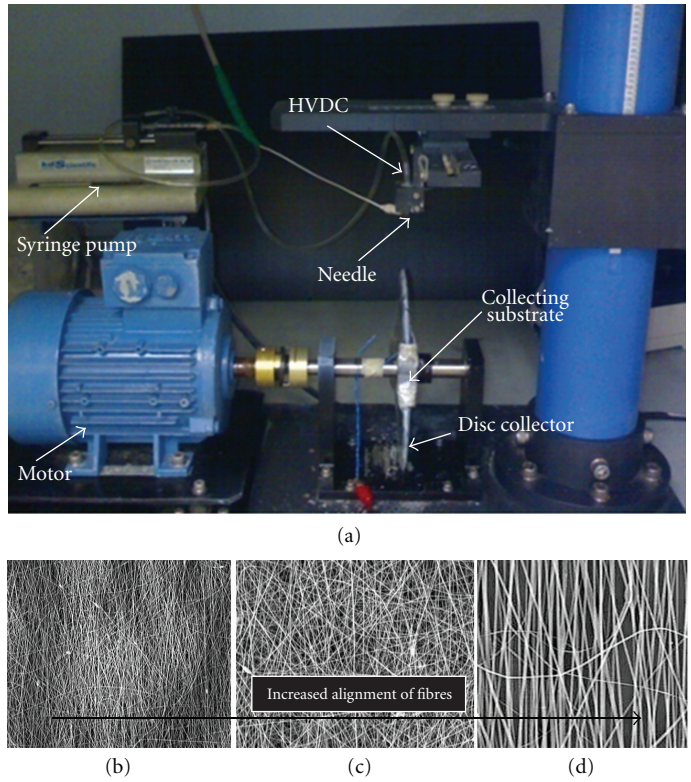

Figure 8: (a) The electrospinning setup for the fabrication of aligned TiO_2 fibers. The increase in the alignment of the fiber was observed with the increase in the rotation speed of the disc collector. The speed of the disc was increased from (b) 800, (c) 1000 to (d) 2000 rpm to obtain aligned fibers. The electrospinning was performed at flow rate of 0.1 mL/h with the applied electric field strength of 1 kV/cm.

Nevertheless, the diameter of the fibers obtained was in submicron range thus reducing the applicability of the fibers obtained. Chuangchote's and Supaphol's [45] collector system consists of dual vertical stainless steel wires as the secondary electrodes with grounded aluminum foil as the primary electrodes as shown in Figure 9(f). These vertical steel wires were mounted along the center line between the tip of the needle system and the grounded aluminum foil. Chuangchote and Supaphol [45] was able to achieve simultaneous collection of aligned fibers between the parallel vertical wires and a random fiber mat on the aluminum foil. Nevertheless, aligned fibers were observed between the vertical wires at short collection times, whereas a further increase in the collection time resulted in random fiber mat. Liu et al. [46] employed external magnetic field in the collector region to achieve aligned fibers as shown in Figure 9(g). It was observed that fiber diameter further decreased due to the application of external applied magnetic field near the surface of collector. The percentage decreases in fiber diameter were found to be least 40% due to the application of external applied magnetic field. Liu et al. [46] also observed highly uniform nanofibers with minimal splitting.

This particular category shown in Figure 10 deals with the setups in which dispensing system of the electrospinning setup is modified to obtain aligned fibers. In one of the setup [47] shown in Figure 10(a), the dispensing system consists of a triangular aluminum tip without any solution supply system. The grounded upright coin act as the collector placed a certain distance away from the triangular tip. The triangular tip is dipped in electrospinning solution to form a small droplet on its tip. When a high voltage is applied to the tip, a bundle of electrospun fibers were then formed between the tip and the collector. Wu et al. [47] successfully fabricated ultralong highly oriented fiber bundles. Nevertheless, as the bending instabilities were totally suppressed, the fiber diameter obtained was in micron range. On the other hand, Rafique et al. [48] configured a collector system comprising a tip collector, and a support plate shown in Figure 10(b). Tip collector is assembled from the grounded wire electrode with wooden holder. The needle system was placed at an angle to the tip collector. By controlling the flow rate, Rafique et al. [48] were able to align individual nanofibers. It was noted that the collector tip resulted in the convergence of electric field lines as in Figure 5(b). This resulted in the dragging of nanofibers to the collect tip. The repelling force between similarly charged fibers resulted in the highly aligned fiber mat. Nevertheless, the fibers obtained were broken with their diameter being in submicron range.

4.2. Rate and Area of Deposition of Electrospun Mat. As mentioned, the electrospun jet follows a spiraling path with increasing radius. This phenomenon results in the deposition area of the order or few square centimeters. It has been

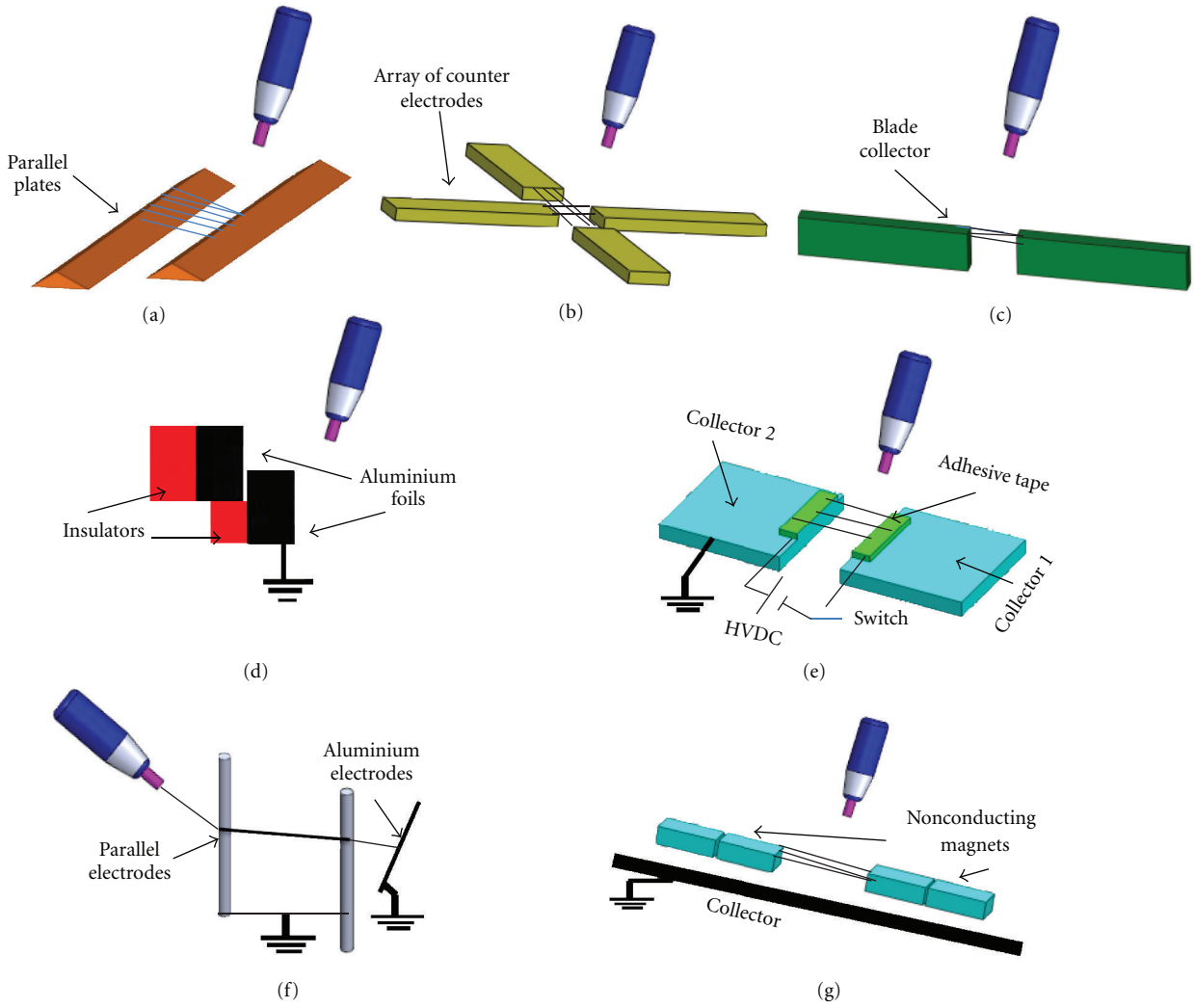

Figure 9: Collector configurations are mainly based upon a group of counter electrodes placed in certain configuration: (a) parallel electrodes: (b) array of counter electrodes: (c) two steel blades placed with a gap: (d) parallel electrode system consisting of aluminum and gold electrodes: (e) two pieces of stainless steel electrodes with the provision to selectively connect to HVDC power supply: (f) collector system consisted of dual vertical stainless steel wires as the secondary electrodes with grounded aluminum foil as the primary electrode: (g) external magnets as auxiliary electrodes.

noticed by the researches that controlling the deposited area and density of electrospun fiber mat will widen the application spectrum of these fibers. Yang et al. [49] designed a regular hexagon distribution multineedle system as shown in Figure 11(a). The setup has the provision of enclosing the needle system inside an iron ring. This particular enclosement helps
in the concentration of electric field lines and thus controlling the deposited area. This multineedle system as expected also increase the deposition density of the fiber mat. On the similar lines, Kim [50] modified the electrospinning setup with the introduction of an electrically charged cylindrical electrode connected to the needle system and a field-controllable target electrode. Both the electrically charged cylindrical electrode and needle system connected to single HVDC supply through a copper wire. Kim [50] noted the convergence of the applied electric field along the spinning axis. This convergence of electric field lines results in a very stable spinning process. The notable feature of the setup was the reduction of the deposited area. This may be due to the suppressing of bending instabilities of electrospun jet by the cylindrical electrode. Due to the application of the field-controllable target electrode, appreciable degree of alignment of nanofibers was also obtained. These field-controllable target electrodes consist of parallel electrodes [50] and circular, interdigitated, and parallel targets [51] connected to HVAC supply. Ying et al. [52] on the other hand controlled the deposition of electrospun fibers by placing an insulating tube around the needle system as shown in Figure 11(b). This is made possible by the static charges developed on the surface of the insulating tube helping in the reduction of the extend of bending instabilities and thus the deposited area. Similar results were obtained by the configuration employing dual rings [53] (Figure 11(d)) and three rings [54] (Figure 11(e))

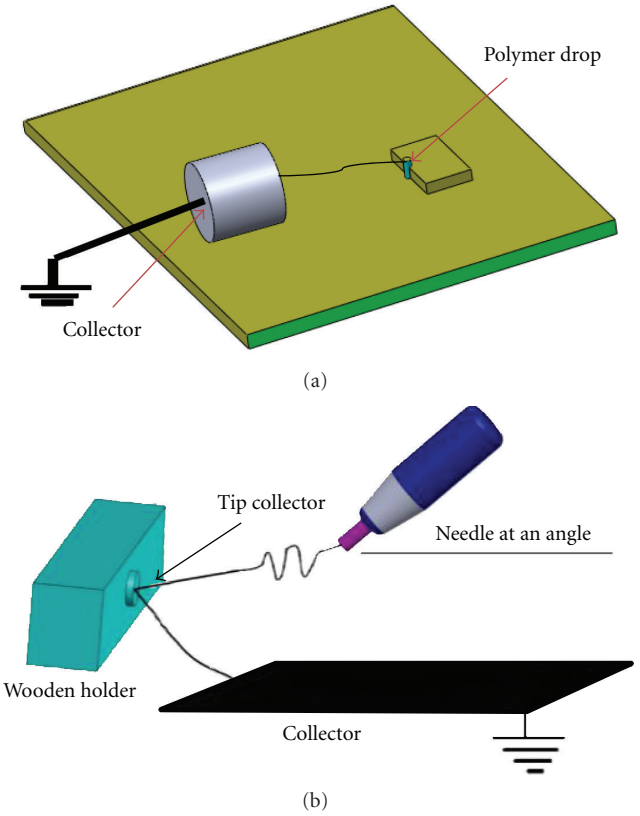

FIGURE 10: This category deals with the setups in which dispensing system of the electrospinning designs is modified to obtain aligned fibers, (a) dispensing system consists of a triangular aluminum tip, (b) needle system was placed at an angle to the tip collector to control the flow rate.

as auxiliary electrodes. Bellan and Craighead [55] employed a group of focusing and steering electrodes placed close to collecting substrate as shown in Figure 11(c). A constant voltage is applied to two focusing electrodes, whereas time-varying voltage is applied to the other two steering electrodes. Employing this setup, Bellan and Craighead [55] were able to focus and steer an electrospinning jet into a patterned structure. Nevertheless, small intricate patterns were not possible due to the limited electronics of the setup.

Li et al. [56] devised 2 needles system with rotating drum as a collector as shown in Figure 11(f). These needle systems were given opposite polarities with respect to each other. This particular configuration resulted in highly intertwined and three-dimensional isotropic network structure. As expected, Li et al. [56] were able to achieve 170 times increase in the throughput compared to the conventional single needle system. Vaseashta [57] was able to achieve a large deposition area by configuring multiple Taylor cone from a single needle system. This is achieved by manipulating the electric field lines near the collector as shown in Figure 11(g). Vaseashta [57] also noted that clogging of the passageway of the needle system from polymer solution may also result in the splitting of the polymer drop and hence formation of more than one Taylor cone. Dosunmu et al. [58] employed porous walled cylindrical tube as the dispensing system depicted in Figure 11(h). In this particular dispensing system, air pressure is applied to push the fluid through the pores. Electrostatic force applied on the drops coming out from the pores resulted in the formation of jets. This particular setup will result in the considerable increase in throughput of the electrospun fibers. Lukas et al. [59] designed a multijet electrospinning setup as shown in Figure 11(i), thus improving the throughput from the process. Lukas et al. [59] observed that sawlike pattern was not the main field concentration, whereas electrospinning jets are created from crests of the exponentially growing wave on the liquid surface.

4.3. Multicomponent Electrospun Fibers. The approach of the modified setup is to produce multicomponent fibers. These components are important for their application in areas such as nanosprings [60], superhydrophobic surfaces [61], sensor [62], and drug delivery [63]. The most prominent in the multicomponent structures are the core-shell structures. These structures may include a core and any number of shells thus resulting in the formation of bicomponent to multicomponent structures. Figure 12(a) depicts the schematic of core-shell structure. The phenomenon mainly comprised of coaxially pumping out two chemically dissimilar solutions. The phenomenon needs precise control of the system and process parameters for achieving core-shell structure. Sun et al. [64] noted that entrainment of nonspinnable core material inside a spinnable shell material is one of the advantages of this particular arrangement. The other variation of this configuration [65] depicted in Figure 12(b) includes gas as a shell material. The gas flow applies additional drawing action on the polymer jet during the electrospinning process. Lin et al. [65] observed a decrease in the fiber diameter with the increase in the gas flow rate. Varesano et al. [66] on other hand, was able to spin crimpled fibers by employing an air flow around a needle system. It was noted that the air flows spiraling downward in the electrospinning chamber impedes the development of the bending instabilities suffered by the electrospun jet. Due to this impeded bending instabilities, Varesano et al. [66] was only able to obtain submicron ranged fibers.

One of the innovative approaches was employed by the Bazilevsky et al. [67] for producing core-shell fibers. Bazilevsky et al. [67] employed a single needle system to electrospin emulsions. It was observed that the dissolved phase undergoes ordinary electrospinning, whereas the dispersion phase gets trapped as a drop at the base of Taylor cone depicted in Figure 12(c). It was observed that the drop stretches due to the force acting on it by the outer fluid. This stretching of drop results in the formation of core-shell fibers. The morphology was also found to be similar to coannular needle electrospinning setups. The other notable configuration designed by Gupta and Wilkes [68] employ dispensing system having two chambers for two given polymer solutions as depicted in Figure 12(d). The dispensing system disperses two solutions from a single needle, thus fabricating bicomponent nanofibers. The other configuration [69] shown in Figure 12(e) includes a rotating drum between two needle systems. Each of these needle systems disperses a desired solution. This configuration allowed for the production

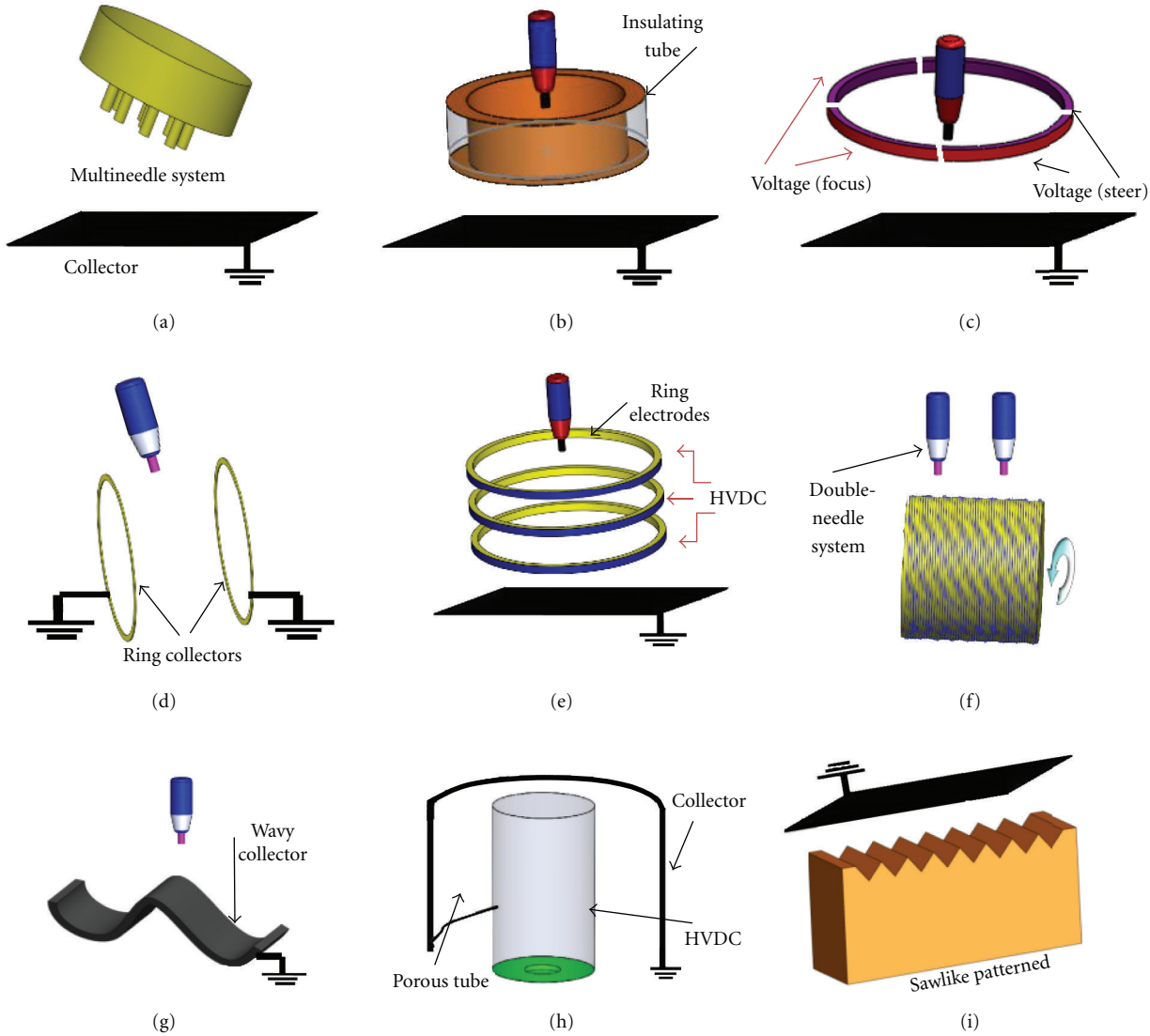

Figure 11: Setups to control the deposited area and density of electrospun fiber, (a) regular hexagon multineedle system enclosed inside an iron ring, (b) insulating tube around the needle system, (c) group of focusing and steering electrodes placed close to collecting substrate, (d) dual rings, (e) three rings, (f) 2-needle system, (g) wavy-shaped collector, (h) porous-walled cylindrical tube as the dispensing system, and (i) sawlike-patterned dispensing system.

of homogeneously mixed superhydrophobic composite nanofibers. Duan et al. [69] on the other hand, was able to configure mechanically stable highly hydrophilic membranes with the similar electrospinning setup.

In-house designed core-shell setup was employed for the production of core-shell as well as hollow fibers shown in Figure 13. These fibers are being employed for the advanced application such as photocathodes in dye-synthesized solar cells, gas sensors, and regenerative medicine applications. Hollow fibers obtained were employed as photocathodes in DSSCs due to their large surface area to the volume ratio. This large surface area of the hollow fibers results in the improved dye loading of the photocathode and thus improved performance of the solar cells. The abovementioned work will appear elsewhere. Work is also in the process to employ core-shell fiber in the solid state solar cells, web guides, gas sensors, and so forth.

Though the core-shell and bicomponent nanofibers are quite promising, the final fiber morphology largely depends upon the fluid dynamics in the boundary layer at the interface of the dissimilar fluid components. A thick boundary layer at the interface will imply a large drag force acting on the inner fluid component. This large drag force will impede the flow of inner fluid component resulting in predominately single component nanofibers, thus defying the purpose of the designed setup. This implies that proper control of process and system parameters such as flow rate and chemical composition of the solutions is required for the production of core-shell fibers.

Composite nanofibers are also being obtained through chemical synthesis by employing electrospun fibers as the base material. For instance, Sebastian et al. [70] (co-researcher at NUSNNI, NUS, Singapore) fabricated efficient catalytic filter membrane employing nanofibers as shown in

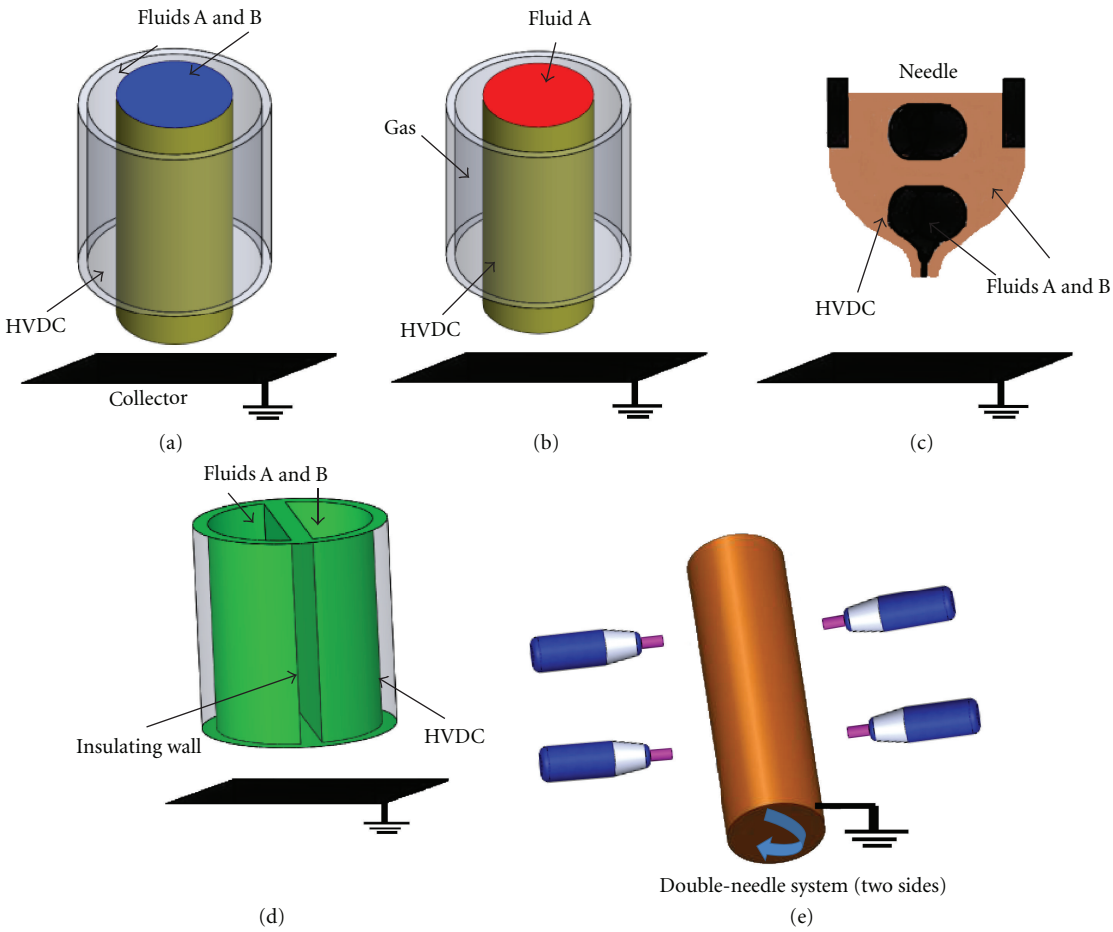

Figure 12: The function of the modified setup is to produce multicomponent fibers, (a) core shell, (b) gas as a shell material in core-shell structure, (c) single-needle core shell structure, (d) bicomponent electrospinning system, and (e) rotating drum between two needle systems as electrospinning setup.

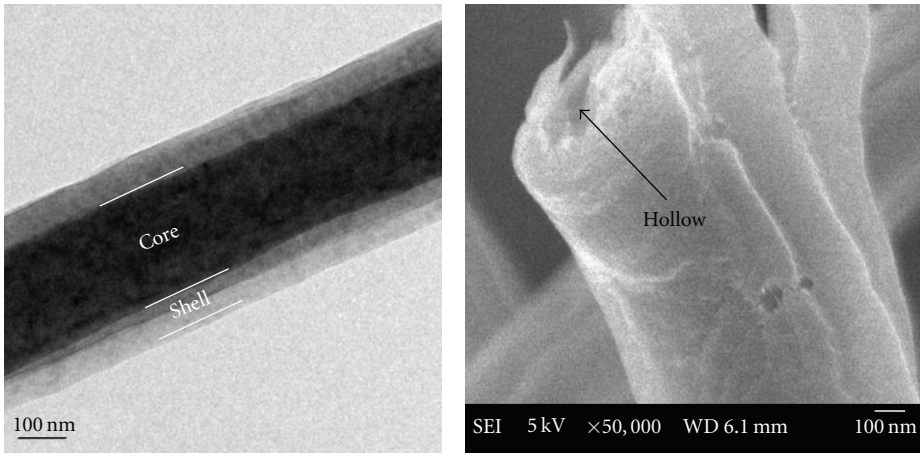

Figure 13: (a) TEM of core-shell fibers prepared by coaxial electrospinning. 10 wt% aqueous polyvinyl alcohol (PVA) was employed as the core, whereas 8 wt% polyvinylpyrrolidone (PVP) dissolved in dimethylformamide (DMF) as the shell. The electrospinning was performed at the applied electric field strength of 1.5 kV/cm, (b) SEM image of the hollow TiO_2 nanofibers.

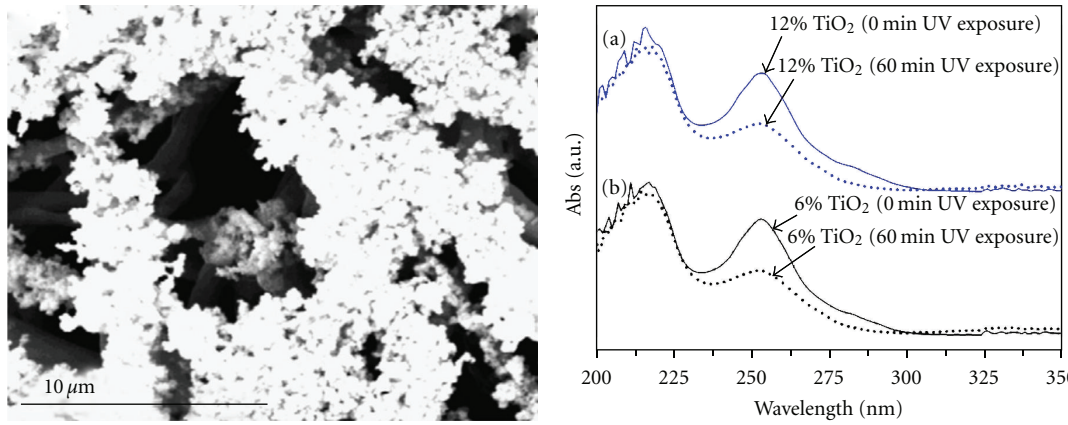

FIGURE 14: (a) TiO_2 nanoparticles deposited on 12 wt% PANi/PEO-blended nanofibrous mat. (b) Increase in the catalytic activity of the composite fiber with the increase in the concentration of the TiO_2 deposited on the conductive PANi/PEO-blended nanofibers.

Figure 14(a). The catalytic filter membrane was fabricated by electrospraying TiO_2 nanoparticles on electrically conductive PANi-PEO nanofibrous membrane. It was noted that blended PANi-PEO nanofibrous membrane as the collecting substrate resulted in the uniform deposition of TiO_2 on its surface as compared to fiber mat placed on aluminum foil. It can be seen from the Figure 14(b) that the catalytic activity of the membrane improved with an increase in the concentration of TiO_2 nanoparticles. The obtained membrane was found to be highly stable against ultrasonic sonication, thus making it viable for large-scale industrial production.

4.4. Yarns. These twisted nanofibers that can emulate organic material such as collagen and DNA are being readily exploited in the field such as tissue engineering [71] to p-n junction [72]. A number of electrospinning configurations are being analyzed related to configuring nanofibrous yarn. One of these configurations shown in Figure 15(a) depicts the phenomenon of self-bundling electrospinning employed for the generation of continuous electrospun yarn. An external electrode is employed to initiate self-bundling of the nanofibers, which is later collected on the rotating mandrel. Wang et al. [73] observed that the conductivity played a major role in the production of continuous self-bundled yarns. It was noted that the increment in the conductivity of the polymer solution resulted in the self-bundling of the fiber without the need of the external electrode. Aggravated bending instability due to the increase in the conductivity of polymer solution was considered responsible for the above phenomenon. The particular setup [74] shown in Figure 15(b) consists of electrospinning nanofibers in a liquid container. This is done to neutralize the free charges available on the surface of the fibers. These neutralized fibers were later collected as the fiber yarn via a rotating mandrel. Gu et al. [75] proposed a novel configuration for the production of yarn shown in Figure 15(c). This setup consists of four auxiliary electrodes with a usual ground electrode. The purpose of these electrodes is to help in the twisting of nanofibers. These electrodes are electrically activated in sequence to allow the 360° rotation of electrospun jet. The yarn was later collected on the grounded surface. Gu et al. [75] were also able to control the twist length of the yarn by controlling the rotation time of the amplitude of electric field on the auxiliary electrode.

The other setup [53] consists of two grounded stainless steel rings placed at a certain distance apart, shown in Figure 15(d). These fibers get suspended between the collector rings. One of these collector rings is allowed to rotate about its axis thus producing twisted nanofibers. This setup though simple results in the low throughput. The other setup [76] depicted in Figure 15(e) consists of two needles systems placed in the horizontal direction facing each other. Each of these needle systems consists of a syringe pump with a HVDC supply. These syringe systems were given opposite polarities with respect to each other. These opposite polarities help in the sticking of the oppositely charged fibers originating from the needles. The fiber yarn thus obtained is considered to be electrically neutral, thus not attracted to any of the electrically charged needles. Pan et al. [76] observed that it was easier to align this electrically neutral yarn with the help of a rotating collector. The shortcoming of this particular setup may be the manual towing of fiber yarn to the rotating collector.

5. Conclusions

Various electrospinning setups have been discussed based on their applications. This is done for the researchers to make a calculated choice regarding design of their electrospinning setup. Four basic categories were identified, namely, patterned fibers, fiber yarns, and multicomponent and rate and area of deposition of electrospun mat. These categories help to analyze the limitations of the electrospinning process, that is, what need to be done to better utilize the inherent capabilities of the electrospinning process? Nevertheless, we hope that this analysis will shed some light on one of the highly researched nanofiber production techniques.

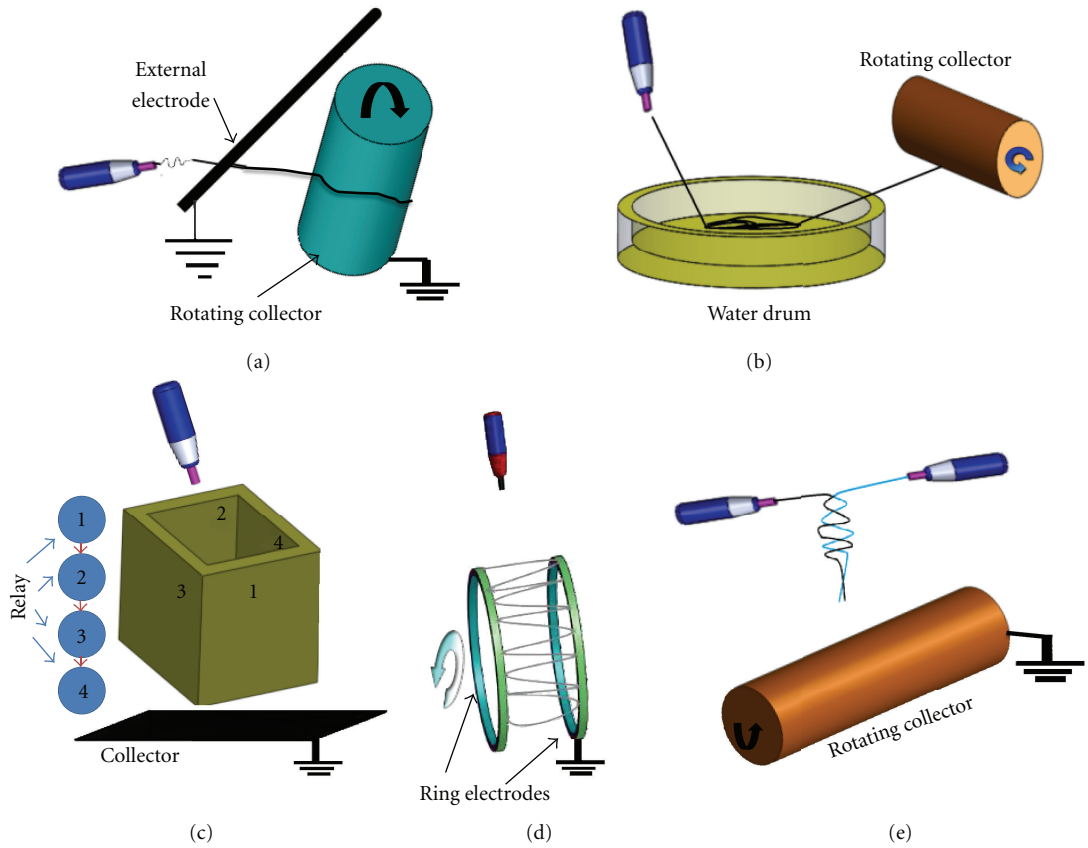

Figure 15: These setups are employed to produce twisted nanofibers, (a) self-bundling electrospinning, (b) electrospinning in a liquid container to neutralize the free charges, (c) twisting by four auxiliary electrodes, (d) ring collector, and (e) two horizontal needles systems.

Acknowledgments

The authors gratefully acknowledge National University of Singapore, Nanyang Technological University, and National Research Foundation, Singapore, for funding support of the research Grant (NRF-CRP-4-2008-03).

References

[1] J. S. Im, S. C. Kang, S. H. Lee, and Y. S. Lee, "Improved gas sensing of electrospun carbon fibers based on pore structure, conductivity and surface modification," *Carbon*, vol. 48, no. 9, pp. 2573–2581, 2010.

[2] J. Yuan, J. Geng, Z. Xing, J. Shen, I. K. Kang, and H. Byun, "Electrospinning of antibacterial poly(vinylidene fluoride) nanofibers containing silver nanoparticles," *Journal of Applied Polymer Science*, vol. 116, no. 2, pp. 668–672, 2010.

[3] S. Y. Chew, R. Mi, A. Hoke, and K. W. Leong, "The effect of the alignment of electrospun fibrous scaffolds on Schwann cell maturation," *Biomaterials*, vol. 29, no. 6, pp. 653–661, 2008.

[4] S. Chuangchote, J. Jitputti, T. Sagawa, and S. Yoshikawa, "Photocatalytic activity for hydrogen evolution of electrospun TiO2 nanofibers," *ACS Applied Materials & Interfaces*, vol. 1, no. 5, pp. 1140–1143, 2009.

[5] Y. C. Ahn, S. K. Park, G. T. Kim et al., "Development of high efficiency nanofilters made of nanofibers," *Current Applied Physics*, vol. 6, no. 6, pp. 1030–1035, 2006.

[6] C. Barrera, K. Hyde, J. P. Hinestroza, T. Gould, G. Montero, and C. Rinaldi, "Electrospun magnetic nanofibers with anti-counterfeiting applications," in *Proceedings of the ASME International Mechanical Engineering Congress and Exposition (IMECE '05)*, pp. 467–473, New York, NY, USA, November 2005.

[7] Y. K. Kang, C. H. Park, J. Kim, and T. J. Kang, "Application of electrospun polyurethane web to breathable water-proof fabrics," *Fibers and Polymers*, vol. 8, no. 5, pp. 564–570, 2007.

[8] M. Grätzel, "Dye-sensitized solid-state heterojunction solar cells," *MRS Bulletin*, vol. 30, no. 1, pp. 23–27, 2005.

[9] R. E. Taylor, "Electrically Driven Jets," *Proceedings—Royal Society of London, A*, vol. 313, pp. 453–475, 1969.

[10] A. F. Spivak and Y. A. Dzenis, "Asymptotic decay of radius of a weakly conductive viscous jet in an external electric field," *Applied Physics Letters*, vol. 73, no. 21, pp. 3067–3069, 1998.

[11] A. F. Spivak, Y. A. Dzenis, and D. H. Reneker, "Model of steady state jet in the electrospinning process," *Mechanics Research Communications*, vol. 27, no. 1, pp. 37–42, 2000.

[12] A. L. Yarin, S. Koombhongse, and D. H. Reneker, "Taylor cone and jetting from liquid droplets in electrospinning of nanofibers," *Journal of Applied Physics*, vol. 90, no. 9, pp. 4836–4846, 2001.

[13] A. L. Yarin, S. Koombhongse, and D. H. Reneker, "Bending instability in electrospinning of nanofibers," *Journal of Applied Physics*, vol. 89, no. 5, pp. 3018–3026, 2001.

[14] M. M. Hohman, M. Shin, G. Rutledge, and M. P. Brenner, "Electrospinning and electrically forced jets. I. Stability theory," *Physics of Fluids*, vol. 13, no. 8, pp. 2201–2220, 2001.

[15] M. M. Hohman, M. Shin, G. Rutledge, and M. P. Brenner, "Electrospinning and electrically forced jets. II. Applications," *Physics of Fluids*, vol. 13, no. 8, pp. 2221–2236, 2001.

[16] J. J. Feng, "The stretching of an electrified non-Newtonian jet: a model for electrospinning," *Physics of Fluids*, vol. 14, no. 11, pp. 3912–3926, 2002.

[17] J. J. Feng, "Stretching of a straight electrically charged viscoelastic jet," *Journal of Non-Newtonian Fluid Mechanics*, vol. 116, no. 1, pp. 55–70, 2003.

[18] C. P. Carroll and Y. L. Joo, "Electrospinning of viscoelastic Boger fluids: modeling and experiments," *Physics of Fluids*, vol. 18, no. 5, Article ID 053102, 14 pages, 2006.

[19] D. H. Reneker, A. L. Yarin, H. Fong, and S. Koombhongse, "Bending instability of electrically charged liquid jets of polymer solutions in electrospinning," *Journal of Applied Physics*, vol. 87, no. 9, pp. 4531–4547, 2000.

[20] A. L. Yarin, W. Kataphinan, and D. H. Reneker, "Branching in electrospinning of nanofibers," *Journal of Applied Physics*, vol. 98, no. 6, Article ID 064501, pp. 1–12, 2005.

[21] L. Huang, K. Nagapudi, P. R. Apkarian, and E. L. Chaikof, "Engineered collagen—PEO nanofibers and fabrics," *Journal of Biomaterials Science, Polymer Edition*, vol. 12, no. 9, pp. 979–993, 2001.

[22] T. Lin, H. Wang, H. Wang, and X. Wang, "The charge effect of cationic surfactants on the elimination of fibre beads in the electrospinning of polystyrene," *Nanotechnology*, vol. 15, no. 9, pp. 1375–1381, 2004.

[23] K. H. Lee, H. Y. Kim, M. S. Khil, Y. M. Ra, and D. R. Lee, "Characterization of nano-structured poly(ε-caprolactone) nonwoven mats via electrospinning," *Polymer*, vol. 44, no. 4, pp. 1287–1294, 2003.

[24] L. Rayleigh, "On the instability of a cylinder of viscous liquid under capillary forces," *Philosophical Magazine Series 5*, vol. 34, no. 207, pp. 145–154, 1982.

[25] H. Fong, I. Chun, and D. H. Reneker, "Beaded nanofibers formed during electrospinning," *Polymer*, vol. 40, no. 16, pp. 4585–4592, 1999.

[26] M. G. McKee, G. L. Wilkes, R. H. Colby, and T. E. Long, "Correlations of solution rheology with electrospun fiber formation of linear and branched polyesters," *Macromolecules*, vol. 37, no. 5, pp. 1760–1767, 2004.

[27] A. L. Yarin and E. Zussman, "Upward needleless electrospinning of multiple nanofibers," *Polymer*, vol. 45, no. 9, pp. 2977–2980, 2004.

[28] S. W. Lee, H. J. Lee, J. H. Choi et al., "Periodic array of polyelectrolyte-gated organic transistors from electrospun poly(3-hexylthiophene) nanofibers," *Nano Letters*, vol. 10, no. 1, pp. 347–351, 2010.

[29] K. J. Aviss, J. E. Gough, and S. Downes, "Aligned electrospun polymer fibres for skeletal muscle regeneration," *European Cells & Materials*, vol. 19, pp. 193–204, 2010.

[30] M. Campoy-Quiles, Y. Ishii, H. Sakai, and H. Murata, "Highly polarized luminescence from aligned conjugated polymer electrospun nanofibers," *Applied Physics Letters*, vol. 92, no. 21, Article ID 213305, 2008.

[31] J. A. Matthews, G. E. Wnek, D. G. Simpson, and G. L. Bowlin, "Electrospinning of collagen nanofibers," *Biomacromolecules*, vol. 3, no. 2, pp. 232–238, 2002.

[32] N. Bhattarai, D. Edmondson, O. Veiseh, F. A. Matsen, and M. Zhang, "Electrospun chitosan-based nanofibers and their cellular compatibility," *Biomaterials*, vol. 26, no. 31, pp. 6176–6184, 2005.

[33] P. Katta, M. Alessandro, R. D. Ramsier, and G. G. Chase, "Continuous electrospinning of aligned polymer nanofibers onto a wire drum collector," *Nano Letters*, vol. 4, no. 11, pp. 2215–2218, 2004.

[34] B. Sundaray, V. Subramanian, T. S. Natarajan, R. Z. Xiang, C. C. Chang, and W. S. Fann, "Electrospinning of continuous aligned polymer fibers," *Applied Physics Letters*, vol. 84, no. 7, pp. 1222–1224, 2004.

[35] W. E. Teo and S. Ramakrishna, "Electrospun fibre bundle made of aligned nanofibres over two fixed points," *Nanotechnology*, vol. 16, no. 9, pp. 1878–1884, 2005.

[36] W. E. Teo, M. Kotaki, X. M. Mo, and S. Ramakrishna, "Porous tubular structures with controlled fibre orientation using a modified electrospinning method," *Nanotechnology*, vol. 16, no. 6, pp. 918–924, 2005.

[37] C. Y. Xu, R. Inai, M. Kotaki, and S. Ramakrishna, "Aligned biodegradable nanofibrous structure: a potential scaffold for blood vessel engineering," *Biomaterials*, vol. 25, no. 5, pp. 877–886, 2004.

[38] E. Zussman, A. Theron, and A. L. Yarin, "Formation of nanofiber crossbars in electrospinning," *Applied Physics Letters*, vol. 82, no. 6, pp. 973–975, 2003.

[39] D. Li, Y. Wang, and Y. Xia, "Electrospinning nanofibers as uniaxially aligned arrays and layer-by-layer stacked films," *Advanced Materials*, vol. 16, no. 4, pp. 361–366, 2004.

[40] D. Li, Y. Wang, and Y. Xia, "Electrospinning of polymeric and ceramic nanofibers as uniaxially aligned arrays," *Nano Letters*, vol. 3, no. 8, pp. 1167–1171, 2003.

[41] S. J. Lee, N. I. Cho, and D. Y. Lee, "Effect of collector grounding on directionality of electrospun titania fibers," *Journal of the European Ceramic Society*, vol. 27, no. 13–15, pp. 3651–3654, 2007.

[42] M. V. Kakade, S. Givens, K. Gardner, K. H. Lee, D. B. Chase, and J. F. Rabolt, "Electric field induced orientation of polymer chains in macroscopically aligned electrospun polymer nanofibers," *Journal of the American Chemical Society*, vol. 129, no. 10, pp. 2777–2782, 2007.

[43] M. K. Shin, S. I. Kim, and S. J. Kim, "Controlled assembly of polymer nanofibers: from helical springs to fully extended," *Applied Physics Letters*, vol. 88, no. 22, 3 pages, 2006.

[44] Y. Ishii, H. Sakai, and H. Murata, "A new electrospinning method to control the number and a diameter of uniaxially aligned polymer fibers," *Materials Letters*, vol. 62, no. 19, pp. 3370–3372, 2008.

[45] S. Chuangchote and P. Supaphol, "Fabrication of aligned poly (vinyl alcohol) nanofibers by electrospinning," *Journal of Nanoscience and Nanotechnology*, vol. 6, no. 1, pp. 125–129, 2006.

[46] Y. Liu, X. Zhang, Y. Xia, and H. Yang, "Magnetic-field-assisted electrospinning of aligned straight and wavy polymeric nanofibers," *Advanced Materials*, vol. 22, no. 22, pp. 2454–2457, 2010.

[47] H. Wu, D. Lin, R. Zhang, and W. Pan, "Oriented nanofibers by a newly modified electrospinning method," *Journal of the American Ceramic Society*, vol. 90, no. 2, pp. 632–634, 2007.

[48] J. Rafique, J. Yu, J. Yu et al., "Electrospinning highly aligned long polymer nanofibers on large scale by using a tip collector," *Applied Physics Letters*, vol. 91, no. 6, Article ID 063126, 3 pages, 2007.

[49] Y. Yang, Z. D. Jia, Q. Li, L. Hou, and Z. C. Guan, "Electrospun uniform fibres with a special regular hexagon distributed multi-needles system," *Journal of Physics: Conference Series*, vol. 142, no. 1, Article ID 012027, pp. 1–6, 2008.

[50] G. H. Kim, "Electrospinning process using field-controllable electrodes," *Journal of Polymer Science, Part B*, vol. 44, no. 10, pp. 1426–1433, 2006.

[51] G. Kim and W. Kim, "Nanofiber spraying method using a supplementary electrode," *Applied Physics Letters*, vol. 89, no. 1, pp. 013111–013111-3, 2006.

[52] Y. Ying, J. Zhidong, and G. Zhicheng, "Controlled deposition of electrospun poly (ethylene oxide) fibers via insulators," in *Proceedings of the 15th IEEE International Conference on Dielectric Liquids (ICDL '05)*, pp. 457–460, Coimbra, Portugal, July 2005.

[53] P. D. Dalton, D. Klee, and M. Möller, "Electrospinning with dual collection rings," *Polymer*, vol. 46, no. 3, pp. 611–614, 2005.

[54] J. M. Deitzel, J. Kleinmeyer, D. Harris, and N. C. Beck Tan, "The effect of processing variables on the morphology of electrospun nanofibers and textiles," *Polymer*, vol. 42, no. 1, pp. 261–272, 2001.

[55] L. M. Bellan and H. G. Craighead, "Control of an electrospinning jet using electric focusing and jet-steering fields," *Journal of Vacuum Science and Technology B*, vol. 24, no. 6, pp. 3179–3183, 2006.

[56] M. Li, Y. D. He, C. L. Xin et al., "Dual electrode mode electrospinning of biodegradable polymers," *Applied Physics Letters*, vol. 92, no. 21, 3 pages, 2008.

[57] A. Vaseashta, "Controlled formation of multiple Taylor cones in electrospinning process," *Applied Physics Letters*, vol. 90, no. 9, Article ID 093115, 3 pages, 2007.

[58] O. O. Dosunmu, G. G. Chase, W. Kataphinan, and D. H. Reneker, "Electrospinning of polymer nanofibres from multiple jets on a porous tubular surface," *Nanotechnology*, vol. 17, no. 4, pp. 1123–1127, 2006.

[59] D. Lukas, A. Sarkar, and P. Pokorny, "Self-organization of jets in electrospinning from free liquid surface: a generalized approach," *Journal of Applied Physics*, vol. 103, no. 8, Article ID 084309, 7 pages, 2008.

[60] C. Shuiliang, H. Haoqing, H. Ping, J. H. Wendorff, A. Greiner, and S. Agarwal, "Polymeric nanosprings by bicomponent electrospinning," *Macromolecular Materials and Engineering*, vol. 294, no. 4, pp. 265–271, 2009.

[61] A. Borras, A. Barranco, and A. R. González-Elipe, "Reversible superhydrophobic to superhydrophilic conversion of Ag@TiO 2 composite nanofiber surfaces," *Langmuir*, vol. 24, no. 15, pp. 8021–8026, 2008.

[62] S.-W. Choi, J. Y. Park, and S. S. Kim, "Synthesis of SnO*2*-ZnO core-shell nanofibers via a novel two-step process and their gas sensing properties," *Nanotechnology*, vol. 20, no. 46, Article ID 465603, 2009.

[63] H. H. Huang, C. L. He, H. S. Wang, and X. M. Mo, "Preparation of core-shell biodegradable microfibers for long-term drug delivery," *Journal of Biomedical Materials Research—Part A*, vol. 90, no. 4, pp. 1243–1251, 2009.

[64] Z. Sun, E. Zussman, A. L. Yarin, J. H. Wendorff, and A. Greiner, "Compound core-shell polymer nanofibers by co-electrospinning," *Advanced Materials*, vol. 15, no. 22, pp. 1929–1932, 2003.

[65] Y. Lin, Y. Yao, X. Yang et al., "Preparation of poly (ether sulfone) nanofibers by gas-jet/electrospinning," *Journal of Applied Polymer Science*, vol. 107, no. 2, pp. 909–917, 2008.

[66] A. Varesano, A. Montarsolo, and C. Tonin, "Crimped polymer nanofibres by air-driven electrospinning," *European Polymer Journal*, vol. 43, no. 7, pp. 2792–2798, 2007.

[67] A. V. Bazilevsky, A. L. Yarin, and C. M. Megaridis, "Co-electrospinning of core-shell fibers using a single-nozzle technique," *Langmuir*, vol. 23, no. 5, pp. 2311–2314, 2007.

[68] P. Gupta and G. L. Wilkes, "Some investigations on the fiber formation by utilizing a side-by-side bicomponent electrospinning approach," *Polymer*, vol. 44, no. 20, pp. 6353–6359, 2003.

[69] B. Duan, L. Wu, X. Yuan et al., "Hybrid nanofibrous membranes of PLGA/chitosan fabricated via an electrospinning array," *Journal of Biomedical Materials Research—Part A*, vol. 83, no. 3, pp. 868–878, 2007.

[70] N. Sebastian, P. Damian, T. Velmurugan, E. Wintermantel, and S. Ramakrishna, "Conductive electrospun PANi-PEO/TiO*2* fibrous membrane for photo catalysis," *Materials Science and Engineering B*, vol. 176, no. 8, 7 pages, 2011.

[71] W. E. Teo, S. Liao, C. K. Chan, and S. Ramakrishna, "Remodeling of three-dimensional hierarchically organized nanofibrous assemblies," *Current Nanoscience*, vol. 4, no. 4, pp. 361–369, 2008.

[72] A. F. Lotus, S. Bhargava, E. T. Bender et al., "Electrospinning route for the fabrication of p-n junction using nanofiber yarns," *Journal of Applied Physics*, vol. 106, no. 1, Article ID 014303, 2009.

[73] X. Wang, K. Zhang, M. Zhu et al., "Continuous polymer nanofiber yarns prepared by self-bundling electrospinning method," *Polymer*, vol. 49, no. 11, pp. 2755–2761, 2008.

[74] E. Smit, U. Buttner, and R. D. Sanderson, "Continuous yarns from electrospun fibers," *Polymer*, vol. 46, no. 8, pp. 2419–2423, 2005.

[75] B. K. Gu, M. K. Shin, K. W. Sohn et al., "Direct fabrication of twisted nanofibers by electrospinning," *Applied Physics Letters*, vol. 90, no. 26, Article ID 263902, 2007.

[76] H. Pan, L. Li, L. Hu, and X. Cui, "Continuous aligned polymer fibers produced by a modified electrospinning method," *Polymer*, vol. 47, no. 14, pp. 4901–4904, 2006.